



Ultrafast photoinduced linear and circular optical anisotropy in the multiferroic hexagonal manganite YMnO_3

M. Pohl,¹ V. V. Pavlov,² I. A. Akimov,^{1,2} V. N. Gridnev,² R. V. Pisarev,² D. R. Yakovlev,^{1,2} and M. Bayer^{1,2}

¹*Experimentelle Physik 2, Technische Universität Dortmund, 44221 Dortmund, Germany*

²*Ioffe Physical-Technical Institute, Russian Academy of Sciences, 194021 St. Petersburg, Russia*

(Received 25 July 2013; revised manuscript received 25 September 2013; published 7 November 2013)

Femtosecond laser spectroscopy is an important tool for investigating fundamental processes of light-matter interaction. Here, we report on transient optical anisotropy in the multiferroic hexagonal manganite YMnO_3 excited by linearly or circularly polarized laser pulses with ~ 17 fs and ~ 34 fs duration. Spectral dependencies of photoinduced optical rotation and ellipticity at different temperatures are analyzed by considering ultrafast population and relaxation processes near the interband transitions from the hybridized $\text{O}(2p)$ - $\text{Mn}(3d)$ to the $\text{Mn}(3d)$ states at photon energies around 1.6 eV. A Raman coherence time of ~ 10 fs between the excited $\Gamma_5 |x\rangle$ and $\Gamma_5 |y\rangle$ states and a relaxation time of ~ 500 fs between the $\Gamma_5 |x,y\rangle$ and $\Gamma_1 |g\rangle$ states for the electronic transition $\Gamma_1 \rightarrow \Gamma_5$ are determined in that way. The ultrashort Raman coherence time is related to the strong electron Coulomb interaction for the $\Gamma_5 |x,y\rangle$ states.

DOI: [10.1103/PhysRevB.88.195112](https://doi.org/10.1103/PhysRevB.88.195112)

PACS number(s): 71.27.+a, 75.50.Ee, 75.78.Jp, 78.47.J-

I. INTRODUCTION

The many $3d$ -transition-metal oxides behaving as Mott insulators are characterized by large on-site Coulomb interactions among the partially filled $3d$ levels and therefore belong to the strongly correlated compounds with intimate connection between their spin, charge, and orbital degrees of freedom.¹⁻³ These materials demonstrate a rich variety of physical phenomena, e.g., high-critical-temperature superconductivity in cuprates, colossal magnetoresistance in manganites, simultaneous coexistence of several order parameters in multiferroics, etc.⁴⁻⁶ There are numerous theoretical and experimental studies of $3d$ -transition-metal oxides with regard to properties such as the electronic structure, electron and hole transport phenomena, magnetic ordering, and optical properties (see, e.g., Refs. 7–9). An important, so far not fully resolved, task is to disclose the physics underlying the interaction of ultrashort laser pulses with strongly correlated systems. There are theories that predict a strong enhancement of the nonlinear optical susceptibility in Mott insulators (see, e.g., Ref. 10). Other theories predict ultrafast dynamics in Mott insulators on time scales of 10–100 fs or even less.^{11,12}

Ultrashort pulsed lasers have opened new opportunities for implementing coherent control of electronic states in matter (see, e.g., Refs. 13–15), which is important for applications in fields as diverse as information processing, optoelectronics,¹⁶ spintronics,¹⁷ biology, and medicine.¹⁸ In this paper, we report on the observation of ultrafast optical anisotropy in the hexagonal manganite YMnO_3 , excited by linearly and circularly polarized femtosecond laser pulses. The observed nonlinear optical phenomena can be attributed to optical alignment and orientation.¹⁹ In conjunction with a theoretical analysis, the experiments enable us to determine an ultrashort relaxation time for the electronic transition $\Gamma_1 \rightarrow \Gamma_5$. This assures that YMnO_3 is an attractive medium for ultrafast nonlinear manipulation of electron states on the femtosecond time scale.

II. HEXAGONAL YMnO_3

Undoped $3d$ -transition-metal oxides are typically good insulators with a rather large optical band gap in the range of

1–4 eV.²⁰ The material of choice for our study is the hexagonal manganite YMnO_3 with point group C_{6v} . It is a multiferroic binary oxide with a ferroelectric Curie temperature $T_C = 913$ K and an antiferromagnetic Néel temperature $T_N = 75$ K.²¹⁻²³ Aside from interesting multiferroic properties (see, e.g., Refs. 24–26), this material also exhibits large second- and third-order optical nonlinearities.²⁷⁻³⁰

During the last decade, the electronic structure of hexagonal rare-earth manganites became a subject of intense theoretical and experimental research. Early *ab initio* calculations predicted an optical band gap of YMnO_3 in the range of ~ 1.5 eV.^{31,32} The top of the valence band is formed by the oxygen $2p$ states strongly hybridized with $3d_{xz}/3d_{yz}$ and $3d_{xy}/3d_{x^2-y^2}$ states. Nevertheless, the oxygen $2p$ states dominate the density of states near the top of the valence band.³³ The hybridization originates from strong noncentrosymmetric distortions of the local symmetry of the six Mn^{3+} ions in the fivefold oxygen coordination in the unit cell of C_{6v} symmetry. First experimental studies reported a presence of a strong optical absorption band near 1.6 eV in the reflection spectrum of LuMnO_3 (Ref. 34) and in polarized ellipsometry spectra in YMnO_3 , ScMnO_3 , and HoMnO_3 .³⁵ Remarkably, it was found that the absorption band at ~ 1.6 eV is strongly polarized and observed only with the incident polarization of the light wave in the xy plane. This observation clearly confirms the electric-dipole character of the observed transition, which definitely may take place only between the states of different symmetries, that is, $2p$ states of the in-plane oxygen ion O^{2-} and $3d$ states of the manganese ion Mn^{3+} . Figure 1(a) shows a schematic energy-level diagram for the optical transition $\Gamma_1 \rightarrow \Gamma_5$ between the hybridized $\text{O}^{2-}(2p)$ - $\text{Mn}^{3+}(3d)$ states and the $\text{Mn}^{3+}(3d_{3z^2-r^2})$ states. The excited state is a doubly degenerate state $\Gamma_5 |x,y\rangle$ for the crystallographic point group C_{6v} .³⁶ Another important feature of the ~ 1.6 eV band is its high oscillator strength, which also confirms this transition being related to states of different symmetries. The most recent first-principles calculations and experimental studies of a large group of hexagonal manganites confirmed this model of the ~ 1.6 eV transition.^{33,37,38} Therefore, in our theoretical model, we treat the ~ 1.6 eV transition in the hexagonal YMnO_3 as

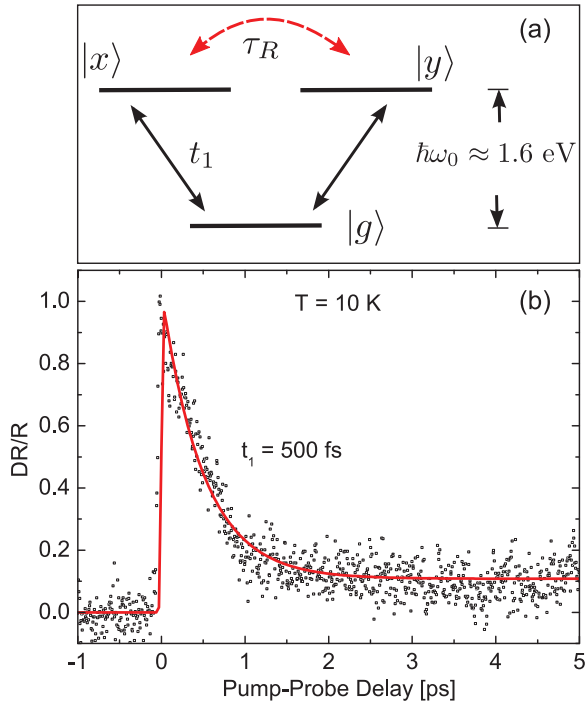


FIG. 1. (Color online) (a) Schematic energy-level diagram for the dipole-allowed optical transition $\Gamma_1 \rightarrow \Gamma_5$ (solid arrows) between the hybridized $O^{2-}(2p)$ - $Mn^{3+}(3d)$ states ($|g\rangle$ is the ground state) and the $Mn^{3+}(3d)$ states ($|x\rangle, |y\rangle$ are the degenerate excited states). The $|x\rangle \rightleftharpoons |y\rangle$ ($|+\rangle \rightleftharpoons |-\rangle$) transitions are characterized by the Raman coherence time τ_R . The $|g\rangle \rightleftharpoons |x,y\rangle$ transitions are characterized by the population relaxation time t_1 . (b) Dynamics of the photoinduced reflectance in $YMnO_3$ for photon energies of 1.55 eV. The points are experimental data, the solid line is a fit to the data with a single exponential convoluted with the pump-probe cross-correlation function.

the interband electric-dipole transition from the hybridized $O(2p)$ - $Mn(3d)$ to the $Mn(3d)$ states.

III. EXPERIMENT

To access the transient nonlinear phenomena, a pump-probe technique was used, in which a linearly or circularly polarized pump beam induces linear or circular optical anisotropy, respectively. In the geometry with the light wave vector parallel to the crystal hexagonal z axis $\mathbf{k} \parallel \mathbf{z}$, the photoinduced changes of the complex dielectric susceptibility tensor of hexagonal manganite $YMnO_3$ can be written as^{39,40}

$$\varepsilon = \begin{pmatrix} \varepsilon_{\perp} + \varepsilon_2 & i\varepsilon_1 & 0 \\ -i\varepsilon_1 & \varepsilon_{\perp} - \varepsilon_2 & 0 \\ 0 & 0 & \varepsilon_{\parallel} \end{pmatrix}, \quad (1)$$

where ε_{\perp} and ε_{\parallel} are the complex dielectric susceptibilities perpendicular and parallel to the crystal hexagonal z axis. ε_1 and ε_2 are the contributions to the dielectric susceptibility tensor ε , induced by the circularly and linearly polarized pump beam, respectively. The photoinduced rotation and ellipticity are related to ε_{\perp} , ε_1 , and ε_2 for circularly polarized

excitation by⁴⁰

$$\theta + i\varepsilon = -\frac{i\varepsilon_1}{\sqrt{\varepsilon_{\perp}(\varepsilon_{\perp} - 1)}}, \quad (2)$$

and for linearly polarized excitation by

$$\theta + i\varepsilon = -\frac{\varepsilon_2 \sin(2\alpha)}{\sqrt{\varepsilon_{\perp}(\varepsilon_{\perp} - 1)}}, \quad (3)$$

where α is the angle between the polarization planes of the linearly polarized pump and probe beams. Linearly polarized light breaks the axial symmetry of a medium and induces a linear optical anisotropy in the xy plane.⁴¹ Therefore, the contribution ε_2 is related to such phenomena as optical alignment,¹⁹ photoselection,⁴² and optical Kerr effect.⁴³ The contribution ε_1 describes the photoinduced circular anisotropy,⁴¹ which is related to optical orientation¹⁹ and inverse Faraday effect.^{43,44} The corresponding magnitude of all these phenomena depends on whether resonant or off-resonant conditions are realized in the experiment.

The pump-probe setup for time-resolved transient measurements including lock-in detection was described earlier.^{45,46} A Ti:sapphire laser generating ultrashort optical pulses with 1.55 eV photon energy at 80 MHz repetition rate was used for optical excitation. The pulse chirp acquired during propagation through the optical elements was compensated by means of a pulse shaper and a compressor using the multiphoton intrapulse interference phase scan (MIIPS) procedure.⁴⁷ The pulse durations of about 17 and 34 fs at the sample position were obtained for spectral widths of 70 and 25 nm, respectively. Subsequently, the laser beam was split into the pump and probe beams, which were focused onto the sample surface to spots of about 20 and 15 μm in diameter, respectively. The pump fluence was about 60 $\mu\text{J}/\text{cm}^2$. Modulation of the pump beam was accomplished by a photoelastic modulator. Depending on the amplitude of modulation, there are two important operation modi at $\lambda/2$ and $\lambda/4$ retardation. These $\lambda/2$ and $\lambda/4$ modi create linearly and circularly polarized pump light, used for measuring either linear or circular photoinduced anisotropy. The signal detection consisted of a Glan-Thompson prism that split the reflected probe beam into two components each sent onto one of the two diodes of a balanced photodetector. This way, a rotation of the polarization plane or a change of the ellipticity angle could be measured with high precision. Polished plane-parallel samples of the hexagonal manganite $YMnO_3$ with their normal along the crystal hexagonal z axis were prepared from flux-grown single crystals. The measurements were done in the temperature range of 10–300 K.

IV. RESULTS

Based on comparison of optical data for different hexagonal manganites, the main spectral feature at 1.6 eV observed by reflectance and ellipsometry techniques^{34,35} is assigned to interband charge-transfer transitions from the oxygen states hybridized strongly with Mn orbitals of different symmetries to the $Mn(3d_{3z^2-r^2})$ state.^{33,38} During excitation of this transition with a photon energy close to the resonance, an electron is moved from the hybridized oxygen-manganese states $O^{2-}(2p)$ - $Mn^{3+}(3d)$ to the manganese $Mn^{3+}(3d)$ states.

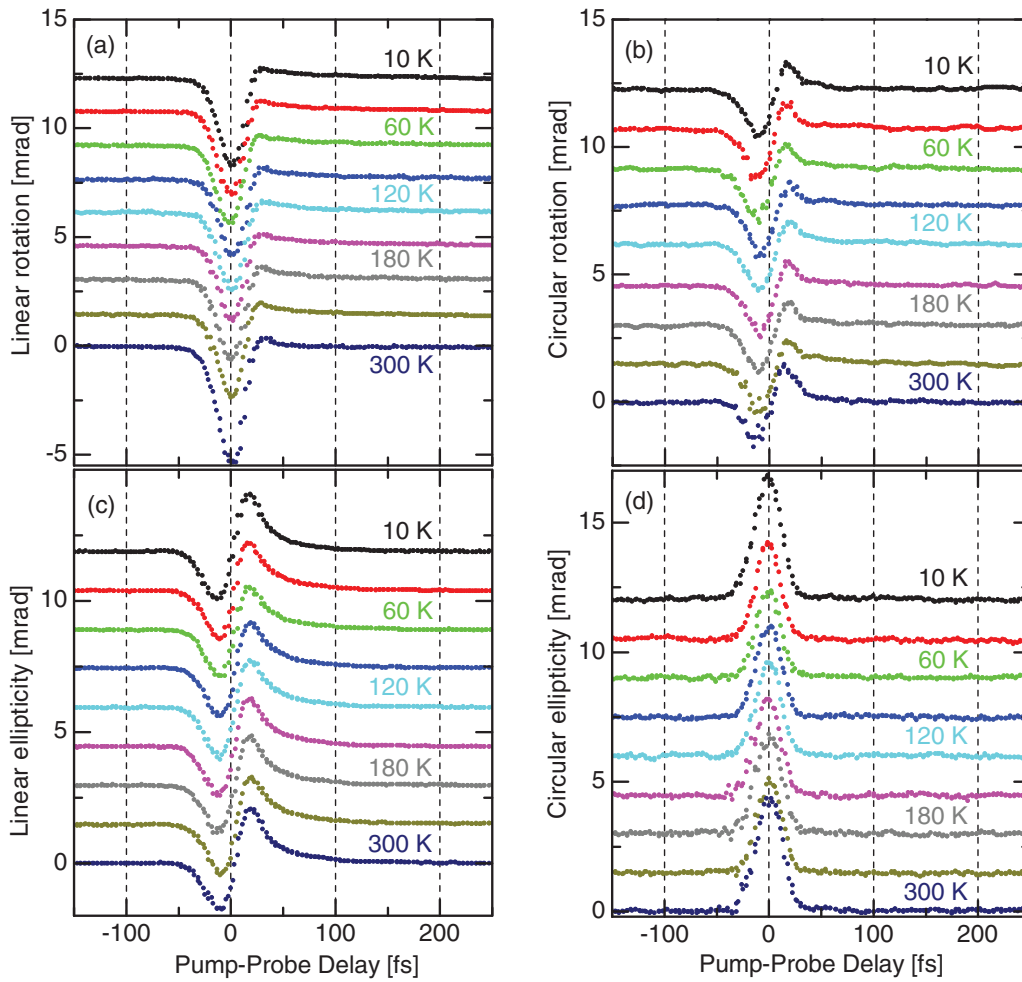


FIG. 2. (Color online) Temporal behavior of the photoinduced rotation and ellipticity for linearly and circularly polarized pump excitation at different temperatures from $T = 10$ up to 300 K.

This process is illustrated in Fig. 1(a) for the electronic transition from the ground nondegenerate state $\Gamma_1 |g\rangle$ to the excited doubly degenerate states with symmetry $\Gamma_5 |x, y\rangle$, and it is in good agreement with the almost 100% polarized optical absorption spectra for linearly polarized light.^{34,35} The lifetime of this transition was measured via the pump-induced differential reflectivity using a conventional chopper modulation at 2 kHz. The result of this experiment is shown in Fig. 1(b). The excited carriers relax with a decay time of ~ 500 fs, which can be well distinguished from the coherent electron dynamics, as will be shown in the following. We note that recently coherent oscillations in the reflectivity signal were found and attributed to acoustic phonon modes at 31 GHz.⁴⁸ These oscillations can not influence the dynamics shown in Fig. 1(b) since they take place on a much longer time scale.

In the pump-probe experiment, a linearly polarized pump beam generates a nonequilibrium electron polarization. Then, the less intense linearly polarized probe with a 45° polarization angle relative to the pump experiences different phase velocities and absorptions for its x and y components, resulting in changes of the optical rotation and ellipticity. This effect will be referred to as photoinduced linear anisotropy. Upon circular excitation by the pump beam, the angular momentum

of the absorbed light is transferred to the medium creating a nonequilibrium electron polarization with nonzero angular momentum. In the following, this effect will be referred to as photoinduced circular anisotropy. The left and right circularly polarized components of the linearly polarized probe beam consequently experience different phase velocities and absorptions, giving rise to circular birefringence and dichroism.⁴⁹

Figure 2 presents results on the temporal behavior of the ultrafast photoinduced linear and circular anisotropy in YMnO_3 at different temperatures. Only small changes of the photoinduced phenomena with respect to the temperature are observed due to a temperature shift of the 1.6 eV absorption band,³⁷ which is comparable with the laser spectral width of ~ 155 meV. We note that the observed photoinduced anisotropy involves only excited states. These states are quite insensitive to the ground electronic states responsible for the antiferromagnetic ordering, therefore ellipticity and rotation signals do not show changes related to the Néel temperature T_N . The dynamical response is faster than 100 fs, i.e., the angular momentum relaxation accessed in this experiment is at least one order of magnitude faster than the carrier relaxation dynamics shown in Fig. 1(b). The signals of

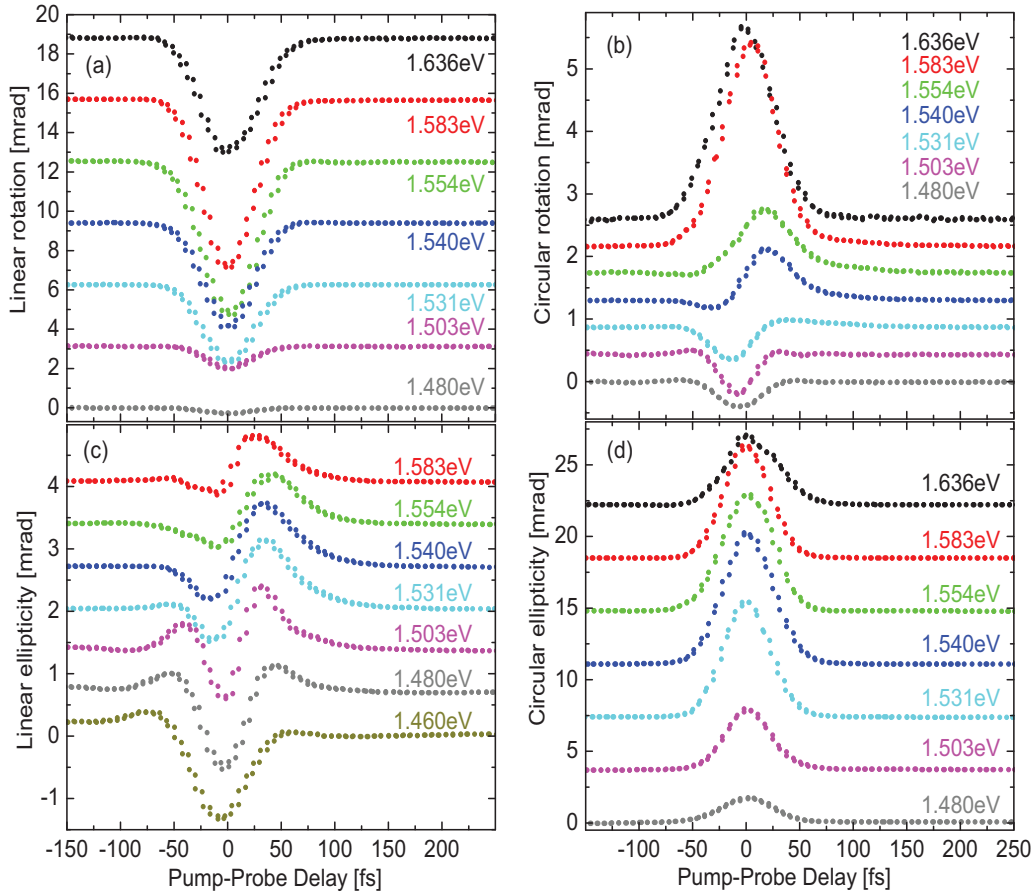


FIG. 3. (Color online) Temporal behavior of the photoinduced rotation and ellipticity for linearly and circularly polarized pump excitation for different photon energies at $T = 300$ K.

linear-induced ellipticity and circular-induced rotation have strongly asymmetric shapes. Consequently, the decay times here are on the order of or shorter than the pulse duration of ~ 17 fs. The signals of linear-induced rotation have only a slightly asymmetric shape, and the temporal behavior of the circular-induced ellipticity is almost symmetric. We note that the observed photoinduced effects are unusually large in comparison with other magnetically ordered materials, where the observation of photoinduced phenomena typically requires use of amplified pulses from titanium-sapphire lasers with laser fluencies on the samples several orders of magnitude larger than for hexagonal YMnO_3 .¹⁴

Figure 3 shows measurements of the pump-probe signals for different photon energies at $T = 300$ K. These measurements were performed using different transmission filters applied to the laser beam, generated by a liquid crystal pulse shaper covering the range of photon energies from 1.460 to 1.636 eV. In this case, the pulse duration time is increased to ~ 34 fs. The resulting changes in temporal dynamics concern only the amplitude of the Gaussian-type signals of the linear-induced rotation and circular-induced ellipticity, showing a maximum around ~ 1.554 and ~ 1.540 eV, respectively. At the same photon energies, the corresponding signals of linear-induced ellipticity and circular-induced rotation both reveal a sign change, which is indicative of a resonant behavior. Moreover, the linear-induced ellipticity shows pronounced features at

negative delay times below 1.531 eV. Since the band structure of the hexagonal manganite YMnO_3 is more complicated in general than the discussed $\text{O}(2p)\text{-Mn}(3d) \rightarrow \text{Mn}(3d)$ transition, the understanding of the origin of the underlying resonance requires a more detailed research.

It is also instructive to compare results on the ultrafast photoinduced linear and circular anisotropy in YMnO_3 for the different pulse durations. Such comparison is presented in Fig. 4, where linear- and circular-induced signals are shown for pulse durations of 17 and 34 fs. The signals of linear-induced ellipticity and circular-induced rotation have a strongly asymmetric shape with a sign change for both pulse durations. On the other hand, the signals of circular-induced ellipticity have symmetric Gaussian shapes, while the signals of linear-induced rotation have a slightly distorted Gaussian shape.

V. DISCUSSION

To describe the dynamical behaviors of the photoinduced linear and circular anisotropy, we model the measured rotation and ellipticity on the basis of the following theoretical considerations. In crystals of the symmetry point group C_{6v} , electric-dipole optical transitions from the ground state Γ_1 are allowed only to the doubly degenerate states of symmetry Γ_5 . In case of a linearly polarized pump, it is convenient

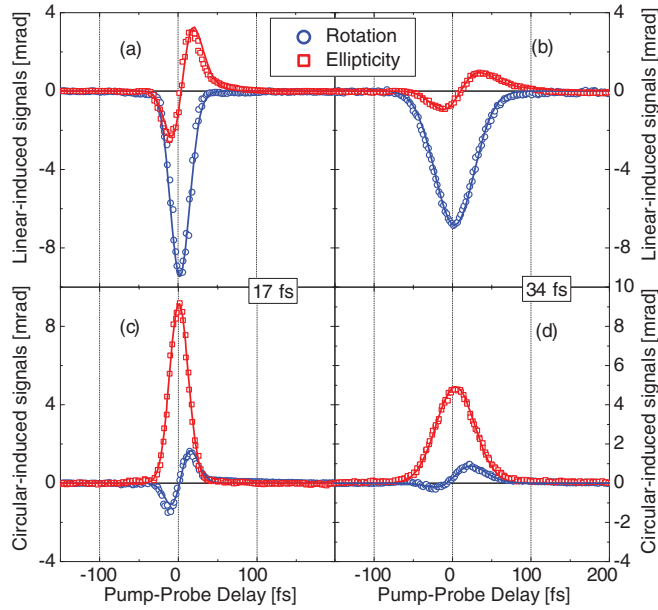


FIG. 4. (Color online) Experimental data on linear- and circular-induced phenomena for pulse duration times of ~ 17 and ~ 34 fs. The temporal behavior of the photoinduced phenomena, calculated on the basis of Eq. (7), is shown by the solid lines.

to choose the wave functions of the excited states in a particular form, $|x\rangle$ and $|y\rangle$, which transform as the Cartesian coordinates x and y under the symmetry operations of the C_{6v} group. The nonzero electric-dipole matrix elements for transitions from the ground state $|g\rangle$ to the excited states $|x\rangle$ and $|y\rangle$ are $\langle g|d_x|x\rangle = \langle g|d_y|y\rangle = d$. The three states $|g\rangle$, $|x\rangle$, and $|y\rangle$ constitute a degenerate three-level system [see Fig. 1(a)].

In the case of a circularly polarized pump, it is convenient to use a circular basis for the wave functions of the excited states:

$$|+\rangle = \frac{1}{\sqrt{2}}(|x\rangle + i|y\rangle), \quad |-\rangle = \frac{1}{\sqrt{2}}(|x\rangle - i|y\rangle), \quad (4)$$

where the states $|\pm\rangle$ are characterized by the z projection J_z of the total angular momentum equal to ± 1 , respectively. The selection rules then give $\langle g|d^+|+\rangle = \langle g|d^-|-\rangle = d$, where $d^\pm = \frac{1}{\sqrt{2}}(d_x \pm id_y)$.

The experimentally measured polarization of the reflected probe pulse is determined by its integral characteristics.⁵⁰ The complex Kerr effect $K = \theta + i\epsilon$ describes the rotation θ and the ellipticity ϵ of the pulse's state of polarization. When a probe pulse linearly polarized along the x axis is reflected at a semi-infinite medium, K is given by^{50,51}

$$K = \frac{2\pi\omega_0}{cI_0} R_0^{-1} \int_0^\infty dz e^{ikz} \int_{-\infty}^\infty dt E_0^*(t) P_y^{(3)}(z,t), \quad (5)$$

where R_0 is the reflection coefficient at the frequency ω_0 , $E_0(t)$ and k are amplitude and wave vector of the probe inside the medium, and $I_0 = \int dt |E_0(t)|^2$ is the integral intensity of the probe pulse.

Since the normal to the sample surface is the sixfold z axis, there is no y component of the reflected probe light for an

incoming x -polarized probe beam in the absence of pumping. Such a component appears only due to the y component of the third-order polarization $\mathbf{P}^{(3)}(t) = \sum_n \mathbf{d}_{0n} \rho_{n0}^{(3)}$ induced by the probe and pump pulses, where \mathbf{d}_{0n} and $\rho_{n0}^{(3)}$ are the matrix elements of the electric-dipole moment and the density matrix, respectively, between the ground and excited states.

In order to calculate the optical rotation and ellipticity from Eq. (5), one needs to know the nonlinear polarization $\mathbf{P}^{(3)}$. This requires solving the Lindblad equation^{52,53}

$$i\hbar \frac{d\hat{\rho}}{dt} = [\hat{H}_0 + \hat{V}, \hat{\rho}] + \hat{R}, \quad (6)$$

where $\hat{\rho}$ is the density matrix, and \hat{H}_0 is the Hamiltonian of the three-level system. \hat{R} describes dissipation leading to decay, $\hat{V} = -\mathbf{d}\mathbf{E}$ represents the interaction with the electric field $\mathbf{E} = \mathbf{E}_p + \mathbf{E}_t$ of the light pulses, where \mathbf{E}_p and \mathbf{E}_t are the fields of the pump and probe, respectively.

Establishing a microscopic understanding would require the solution of Eq. (5) by means of Eq. (6) with the full Hamiltonian. This is beyond the scope of this paper. Therefore, we solve Eq. (5) phenomenologically for the three-level system shown in Fig. 1(a). When approximating the relaxation of the photoinduced angular momentum by a superposition of an exponential and an instantaneous contribution to the decay process and assuming the pump and probe pulses to have Gaussian temporal shapes, the following analytical expression is found for the rotation θ and ellipticity ϵ (Refs. 46 and 54):

$$\theta + i\epsilon = A \exp\left(-\frac{t^2}{\sigma^2}\right) + B \exp\left(\frac{\sigma^2}{4\tau_R^2} - \frac{t}{\tau_R}\right) \times \left[1 - \operatorname{erf}\left(\frac{\sigma}{2\tau_R} - \frac{t}{\sigma}\right)\right], \quad (7)$$

where t is the pump-probe time delay, erf is the Gauss error function, $\sigma = \tau_D/\sqrt{2 \ln 2}$, and τ_D is the full width at half maximum (FWHM) of the Gaussian pulse. The complex coefficients A and B are functions of ϵ_\perp , ϵ_1 , and ϵ_2 [see Eqs. (2) and (3)].

In this model, two relaxation times are used to describe the photoinduced phenomena for electric-dipole optical transitions from the ground state $\Gamma_1 |g\rangle$ to the doubly degenerate states $\Gamma_5 |x, y\rangle$. The relaxation between the excited states $|x\rangle$, $|y\rangle$ and the ground state $|g\rangle$ is characterized by the population relaxation time $t_1 = 500$ fs, as determined from the photoinduced reflectance measurements in YMnO_3 [see Fig. 1(b)]. A pump pulse creates a coherent superposition of the states $|x\rangle$, $|y\rangle$ ($|+\rangle$, $|-\rangle$), and the transitions $|x\rangle \leftrightarrow |y\rangle$ ($|+\rangle \leftrightarrow |-\rangle$) are characterized by a coherence time τ_R . This coherence is therefore commonly referred to as the Raman coherence⁵⁵ and decays with the characteristic time τ_R called the Raman coherence time. Since the states $|+\rangle$, $|-\rangle$ are characterized by the projections of the total angular momentum on the z axis $J_z = +1, -1$, respectively, the time τ_R characterizes in our model the relaxation time of J_z .

The Raman coherence time τ_R can be obtained by fitting the measured signals with Eq. (7), where σ is determined by the experimentally obtained pulse width, the coefficients A , B and the time τ_R are fitting parameters. Using this procedure, the Raman coherence time is determined to $\tau_R = (10 \pm 4)$ fs for both experiments with pulse durations of 17 and 34 fs.

The calculated dependencies for the temporal behavior of the photoinduced phenomena, shown in Fig. 4 by the lines, are in good quantitative agreement with the experimental data, both for linearly and circularly polarized excitation. The temporal evolutions of linear-induced rotation and circular-induced ellipticity have symmetric Gaussian shapes, whereas the linear-induced ellipticity and circular-induced rotation have non-Gaussian shapes. These experimental findings are well reproduced by our theoretical model.

The interband transitions from the hybridized O($2p$)-Mn($3d$) to the Mn($3d$) states at 1.6 eV are characterized by a large on-site Coulomb attraction and lead to the formation of strongly coupled small-sized excitons. The very short Raman coherence time $\tau_R \sim 10$ fs is related to the strong electron Coulomb interaction for the excited $|x\rangle$ and $|y\rangle$ states, and is in line with the rather broad optical absorption band $\Gamma_1 \rightarrow \Gamma_5$ of ~ 0.2 eV.^{34,35} Although the microscopic origin of the bandwidth is still under debate,³⁸ we were able to evaluate the Raman coherence time τ_R in a direct pump-probe experiment.

VI. CONCLUSIONS

The ultrafast photoinduced anisotropy in the Mott insulator YMnO₃ has been observed on a very short time scale. The

nonthermal electron distribution is induced by linearly or circularly polarized pump pulses with subsequent spontaneous decay. The relaxation time hierarchy including the population relaxation time $t_1 = 500$ fs and the Raman coherence time $\tau_R = (10 \pm 4)$ fs has been disclosed. According to our theoretical model, the observed ultrafast dynamics is related to photoexcitation of the dipole-allowed optical transition $\Gamma_1 \rightarrow \Gamma_5$ between the ground state $|g\rangle$ and the excited degenerate states $|x\rangle$, $|y\rangle$ with subsequent relaxation between the excited states carrying the Raman coherence. This relaxation is characterized by the ultrashort time $\tau_R = (10 \pm 4)$ fs due to the strong electron Coulomb interaction. Ultrafast photoinduced phenomena, as observed here at room temperature in the hexagonal manganite YMnO₃, may have a large application potential, because this material can be used for femtosecond laser manipulation of electron states in all-optical device technologies.⁵⁶

ACKNOWLEDGMENTS

This work was supported by the Deutsche Forschungsgemeinschaft, the Russian Foundation for Basic Research (13-02-00754), the Government of the Russian Federation (14.B25.31.0025). V.V.P. thanks the Alexander-von-Humboldt Foundation.

-
- ¹N. F. Mott, *Proc. Phys. Soc., London, Sect. A* **62**, 416 (1949).
²J. Hubbard, *Proc. R. Soc. London, Ser. A* **277**, 237 (1964).
³P. W. Anderson, *Phys. Rev.* **115**, 2 (1959).
⁴P. A. Lee, N. Nagaosa, and X.-G. Wen, *Rev. Mod. Phys.* **78**, 17 (2006).
⁵M. Fiebig, *J. Phys. D: Appl. Phys.* **38**, R123 (2005).
⁶W. Eerenstein, N. D. Mathur, and J. F. Scott, *Nature (London)* **442**, 759 (2006).
⁷M. A. Kastner, R. J. Birgeneau, G. Shirane, and Y. Endoh, *Rev. Mod. Phys.* **70**, 897 (1998).
⁸M. Imada, A. Fujimori, and Y. Tokura, *Rev. Mod. Phys.* **70**, 1039 (1998).
⁹M. B. Salamon and M. Jaime, *Rev. Mod. Phys.* **73**, 583 (2001).
¹⁰G. P. Zhang, *Phys. Rev. Lett.* **86**, 2086 (2001).
¹¹R. Gómez-Abal, O. Ney, K. Satitkovitchai, and W. Hübner, *Phys. Rev. Lett.* **92**, 227402 (2004).
¹²A. Takahashi, H. Gomi, and M. Aihara, *Phys. Rev. B* **69**, 075116 (2004).
¹³A. J. Ramsay, *Semicond. Sci. Technol.* **25**, 103001 (2010).
¹⁴A. Kirilyuk, A. V. Kimel, and T. Rasing, *Rev. Mod. Phys.* **82**, 2731 (2010).
¹⁵Y. Zhang, Z. Nie, and M. Xiao, *Coherent Control of Four-Wave Mixing* (Springer, Beijing, 2011).
¹⁶T. Kamiya, *Femtosecond Technology: From Basic Research to Application Prospects* (Springer, Berlin, 1999).
¹⁷I. Žutić, J. Fabian, and S. Das Sarma, *Rev. Mod. Phys.* **76**, 323 (2004).
¹⁸W. Sibbett, A. A. Lagatsky, and C. T. A. Brown, *Opt. Express* **20**, 6989 (2012).
¹⁹F. Meier and B. P. Zakharchenya, *Optical Orientation* (Elsevier, Amsterdam, 1984).
²⁰J. Zaanen, G. A. Sawatzky, and J. W. Allen, *Phys. Rev. Lett.* **55**, 418 (1985).
²¹G. A. Smolenskii and I. E. Chupis, *Sov. Phys. Usp.* **25**, 475 (1982).
²²S. Lee, A. Pirogov, M. Kang, K.-H. Jang, M. Yonemura, T. Kamiyama, S.-W. Cheong, F. Gozzo, N. Shin, H. Kimura *et al.*, *Nature (London)* **451**, 805 (2008).
²³C.-Y. Ren, *Phys. Rev. B* **79**, 125113 (2009).
²⁴M. Fiebig, T. Lottermoser, D. Fröhlich, A. V. Goltsev, and R. V. Pisarev, *Nature (London)* **419**, 818 (2002).
²⁵B. B. Van Aken, T. T. M. Palstra, A. Filippetti, and N. A. Spaldin, *Nat. Mater.* **3**, 164 (2004).
²⁶P. A. Sharma, J. S. Ahn, N. Hur, S. Park, S. B. Kim, S. Lee, J.-G. Park, S. Guha, and S.-W. Cheong, *Phys. Rev. Lett.* **93**, 177202 (2004).
²⁷D. Fröhlich, S. Leute, V. V. Pavlov, and R. V. Pisarev, *Phys. Rev. Lett.* **81**, 3239 (1998).
²⁸M. Fiebig, D. Fröhlich, K. Kohn, S. Leute, T. Lottermoser, V. V. Pavlov, and R. V. Pisarev, *Phys. Rev. Lett.* **84**, 5620 (2000).
²⁹A. V. Kimel, R. V. Pisarev, F. Bentivegna, and T. Rasing, *Phys. Rev. B* **64**, 201103 (2001).
³⁰Y. T. Wang, C. W. Luo, and T. Kobayashi, *Adv. Condens. Matter Phys.* **2013**, 104806 (2013).
³¹J. E. Medvedeva, V. I. Anisimov, M. A. Korotin, O. N. Mryasov, and A. J. Freeman, *J. Phys.: Condens. Matter* **12**, 4947 (2000).
³²M. Qian, J. Dong, and D. Y. Xing, *Phys. Rev. B* **63**, 155101 (2001).
³³W. S. Choi, D. G. Kim, S. S. A. Seo, S. J. Moon, D. Lee, J. H. Lee, H. S. Lee, D.-Y. Cho, Y. S. Lee, P. Murugavel *et al.*, *Phys. Rev. B* **77**, 045137 (2008).
³⁴A. B. Souchkov, J. R. Simpson, M. Quijada, H. Ishibashi, N. Hur, J. S. Ahn, S. W. Cheong, A. J. Millis, and H. D. Drew, *Phys. Rev. Lett.* **91**, 027203 (2003).

- ³⁵A. M. Kalashnikova and R. V. Pisarev, *JETP Lett.* **78**, 143 (2003).
- ³⁶G. F. Koster, J. O. Dimmock, R. G. Wheeler, and H. Statz, *Properties of the Thirty-two Point Groups* (MIT Press, Cambridge, MA, 1963).
- ³⁷W. S. Choi, S. J. Moon, Sung Seok A. Seo, D. Lee, J. H. Lee, P. Murugavel, T. W. Noh, and Y. S. Lee, *Phys. Rev. B* **78**, 054440 (2008).
- ³⁸A. S. Moskvina and R. V. Pisarev, *Low Temp. Phys.* **36**, 489 (2010).
- ³⁹P. S. Pershan, *J. Appl. Phys.* **38**, 1482 (1967).
- ⁴⁰F. J. Kahn, P. S. Pershan, and J. P. Remeika, *Phys. Rev.* **186**, 891 (1969).
- ⁴¹G. G. Kozlov, E. B. Aleksandrov, and V. S. Zapasskii, *Opt. Spectrosc.* **97**, 909 (2004).
- ⁴²J. Michl and E. W. Thulstrup, *Spectroscopy with Polarized Light: Solute Alignment by Photoselection, Liquid Crystal, Polymers, and Membranes*, Corrected Software Edition (Wiley, Hoboken, NJ, 1995).
- ⁴³Y. R. Shen, *The Principles of Nonlinear Optics* (Wiley, Hoboken, NJ, 2003).
- ⁴⁴P. S. Pershan, J. P. van der Ziel, and L. D. Malmstrom, *Phys. Rev.* **143**, 574 (1966).
- ⁴⁵A. V. Kimel, V. V. Pavlov, R. V. Pisarev, V. N. Gridnev, F. Bentivegna, and T. Rasing, *Phys. Rev. B* **62**, R10610 (2000).
- ⁴⁶V. V. Pavlov, R. V. Pisarev, V. N. Gridnev, E. A. Zhukov, D. R. Yakovlev, and M. Bayer, *Phys. Rev. Lett.* **98**, 047403 (2007).
- ⁴⁷B. Xu, J. M. Gunn, J. M. D. Cruz, V. V. Lozovoy, and M. Dantus, *J. Opt. Soc. Am. B* **23**, 750 (2006).
- ⁴⁸K.-J. Jang, H.-g. Lee, S. Lee, J. Ahn, J. S. Ahn, N. Hur, and S.-W. Cheong, *Appl. Phys. Lett.* **97**, 031914 (2010).
- ⁴⁹A. K. Zvezdin and V. A. Kotov, *Modern Magneto-optics and Magneto-optical Materials*, 1st ed. (Taylor & Francis, New York, 1997).
- ⁵⁰I. A. Yugova, M. M. Glazov, E. L. Ivchenko, and A. L. Efros, *Phys. Rev. B* **80**, 104436 (2009).
- ⁵¹V. N. Gridnev, *JETP Lett.* **93**, 161 (2011).
- ⁵²M. O. Scully, *Quantum Optics* (Cambridge University Press, Cambridge, UK, 1997).
- ⁵³T. Meier, P. Thomas, and S. W. Koch, *Coherent Semiconductor Optics: From Basic Concepts to Nanostructure Applications* (Springer, Berlin, 2007).
- ⁵⁴A. V. Kimel, F. Bentivegna, V. N. Gridnev, V. V. Pavlov, R. V. Pisarev, and T. Rasing, *Phys. Rev. B* **63**, 235201 (2001).
- ⁵⁵K. B. Ferrio and D. G. Steel, *Phys. Rev. Lett.* **80**, 786 (1998).
- ⁵⁶O. Wada, *New J. Phys.* **6**, 183 (2004).